Celora *et al. Molecular Brain* (2023) 16:49
https://doi.org/10.1186/s13041-023-01031-z

Molecular Brain

MICRO REPORT Open Access

# Regulation of dendritic spine length in corticopontine layer V pyramidal neurons by autism risk gene β3 integrin

Lucia Celora[1†], Fanny Jaudon[1,2†], Carmela Vitale[3] and Lorenzo A. Cingolani[1,3*]

**Abstract**

The relationship between autism spectrum disorder (ASD) and dendritic spine abnormalities is well known, but it is unclear whether the deficits relate to specific neuron types and brain regions most relevant to ASD. Recent genetic studies have identified a convergence of ASD risk genes in deep layer pyramidal neurons of the prefrontal cortex. Here, we use retrograde recombinant adeno-associated viruses to label specifically two major layer V pyramidal neuron types of the medial prefrontal cortex: the commissural neurons, which put the two cerebral hemispheres in direct communication, and the corticopontine neurons, which transmit information outside the cortex. We compare the basal dendritic spines on commissural and corticopontine neurons in WT and KO mice for the ASD risk gene *Itgb3*, which encodes for the cell adhesion molecule β3 integrin selectively enriched in layer V pyramidal neurons. Regardless of the genotype, corticopontine neurons had a higher ratio of stubby to mushroom spines than commissural neurons. β3 integrin affected selectively spine length in corticopontine neurons. Ablation of β3 integrin resulted in corticopontine neurons lacking long (> 2 µm) thin dendritic spines. These findings suggest that a deficiency in β3 integrin expression compromises specifically immature spines on corticopontine neurons, thereby reducing the cortical territory they can sample. Because corticopontine neurons receive extensive local and long-range excitatory inputs before relaying information outside the cortex, specific alterations in dendritic spines of corticopontine neurons may compromise the computational output of the full cortex, thereby contributing to ASD pathophysiology.

**Keywords** *Itgb3*, Medial prefrontal cortex, ASD, Dendritic spines, Retrograde labelling

## Main text

While dendritic spine abnormalities are a hallmark of many forms of autism spectrum disorder (ASD; [1]), it is generally not known whether these deficits correlate with brain regions and neuron types most relevant to ASD. Human genetic studies have consistently identified a convergence of ASD risk genes in deep layer pyramidal neurons of the prefrontal cortex [2]. Two major types of pyramidal neurons, with divergent functions, are found intermingled in the deep cortical layer V (LV) of the medial prefrontal cortex (mPFC). Intratelencephalic neurons, whose axons project only within the telencephalon,

†Lucia Celora and Fanny Jaudon contributed equally to this study.

*Correspondence:
Lorenzo A. Cingolani
lcingolani@units.it
[1]Department of Life Sciences, University of Trieste, Trieste 34127, Italy
[2]IRCCS Ospedale Policlinico San Martino, Genoa 16132, Italy
[3]Center for Synaptic Neuroscience and Technology (NSYN), Fondazione Istituto Italiano di Tecnologia (IIT), Genoa 16132, Italy

including the contralateral cortex (commissural [COM] neurons) and pyramidal tract neurons, whose axons remain ipsilateral within the telencephalon and project to distant subcerebral regions, including the pons (corticopontine [CP] neurons; Fig. 1A; [3]). While the dendritic arborization, neuromodulation and electrophysiological properties of COM and CP neurons have been extensively investigated, technical difficulties in differentially labeling them have so far precluded a comparative analysis of their dendritic spines. Likewise, we do not know whether ASD risk genes affect dendritic spines on both types of neurons or only on one of them, thereby skewing how LV cortical circuits integrate synaptic inputs.

Here we used retrograde recombinant adeno-associated viruses (retro-rAAVs; [4] injected into the contralateral cortex or pons to label unambiguously COM or CP neurons, respectively (Fig. 1B). This allowed us to address two questions: First, are density and morphology of basal dendritic spines different between COM and CP neurons? Second, are these spines abnormal in KO mice for the ASD risk gene β3 integrin (*Itgb3*)? We focused on *Itgb3* KO mice because (i) the cell adhesion molecule β3 integrin is enriched in human and mouse LV pyramidal neurons [5, 6], (ii) its association to ASD is supported by both single nucleotide polymorphisms and rare mutations [7], (iii) *Itgb3* KO mice exhibit autism-like behaviors [8] and (iv) members of the integrin family have previously been shown to be important for synaptic plasticity and dendritic spine dynamics [9, 10].

Regardless of the genotype, dendritic spine density was slightly but significantly higher in CP than in COM neurons (Fig. 1C and S1A). This prompted us to investigate whether there were differences in the distribution and density of specific spine subtypes. We therefore classified dendritic spines into three categories (thin, stubby and mushroom), according to morphological criteria (Fig S1E). Compellingly, CP neurons had a higher ratio of stubby to mushroom spines than COM neurons (Fig. 1D), and this was mainly due to a higher density of stubby spines in CP neurons (Fig. 1E and S1C, D). Albeit more pronounced in *Itgb3* KO mice, the differences between neuronal types were present also in WT mice, and were therefore unlikely due to β3 integrin. Notably, the change in the relative distribution between mushroom and stubby spines (which do and do not have visible spine necks, respectively) was also evident in individual dendrites as a spine neck 'kink' in the transversal fluorescence profiles of straighten dendrites in COM but not CP neurons (Fig. 1C). No difference was instead detected in the relative percentage or density of thin spines between neuron types or genotypes (Fig. 1C, D and S1B).

The functional role of stubby spines is debated. While they have traditionally been seen as immature spines, recent studies indicate that a large proportion of stubby spines could be a form of potentiated mushroom spines with very short necks [11]. Regardless, our findings suggest that the number of spines with short and large necks, thus having low diffusional coupling between spine head and parental dendrite, is higher in CP than COM neurons.

β3 integrin affected selectively spine length in CP but not COM neurons. Specifically, ablation of β3 integrin shortened overall spine length in CP neurons, with the effect being largely due to a reduction in the length of thin spines (Fig. 1C, F, S2). Notably, CP KO neurons did not uniformly scale down the length of thin dendritic spines but were most deficient in thin spines longer than ~2 μm (Fig. 1C, G, S2). Because length and head width of dendritic spines were highly heterogeneous, even within each dendritic spine subtype (Fig S2), we examined the distributions of the ratio between spine length and head width, which were found to be positively skewed. We therefore plotted histograms of the logarithm of the spine length to head width ratio, which revealed log-normal distributions of this morphological parameter across spine subtypes (Fig. 1H, S2). Parametric statistical analyses of the transformed data confirmed the specific effect of β3 integrin on thin spines of CP neurons (Fig. 1H, S2).

Taken together, our findings suggest that a deficiency in the ASD risk gene β3 integrin compromises preferentially immature thin spines on CP neurons. Because these are dynamic spines that explore the area surrounding their parental dendrite before forming stable synaptic contacts [1], loss of β3 integrin may reduce the ability of CP neurons to do so, potentially altering their final choice for synaptic partners. Recent data indicate that β3 integrin may have an early, rather than late, function in dendritogenesis [12]. Likewise, this integrin is specifically required for the initiation of neuronal differentiation in neuroblastoma N2a cells [13]. Thus, β3 integrin could play a similar role in CP neurons by promoting spine elongation, because it generates traction forces at adhesion contacts of thin spines, or by preventing spine retraction, because it contributes to the initial and dynamic contacts between synaptic partners. This is reminiscent of the role played by β1 integrin, which maintains immature spines of primary hippocampal neurons in a highly dynamic state by interacting with the cell adhesion molecule telencephalin [14]. A limitation of our study is that we analyzed only dendritic spines on basal dendrites since retrograde labeling prevented us from determining whether apical dendrites in layers I-III originated exclusively from CP or COM neurons of LV. Long-range excitatory inputs to basal dendrites in LV are biased towards CP or COM neurons: inputs from the contralateral cortex and basolateral amygdala target preferentially CP neurons while those from the ventral hippocampus are biased towards COM neurons. Local connectivity is

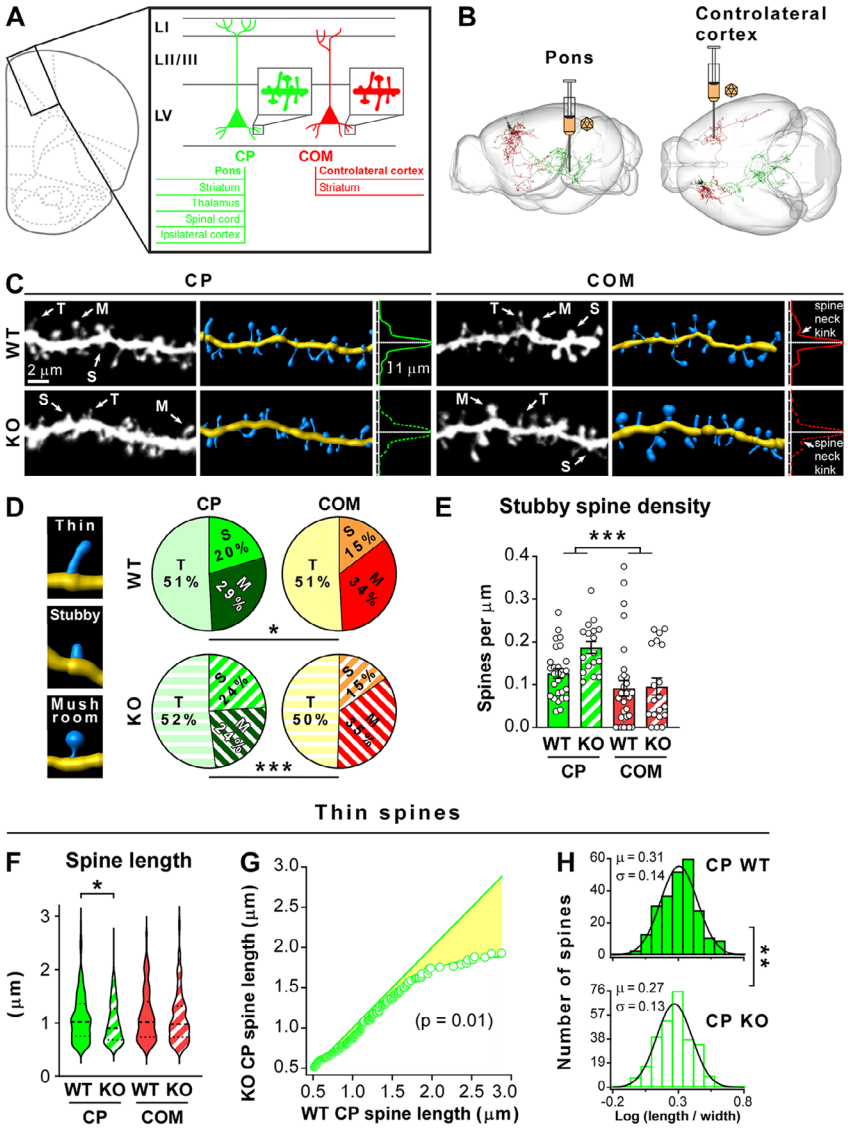


**Fig. 1** Corticopontine but not commissural layer V pyramidal neurons exhibit shorter thin dendritic spines in *Itgb3* KO mice **(A)** Major outputs of LV mPFC pyramidal neurons include the pons for pyramidal tract neurons (corticopontine [CP] neurons; green) and the contralateral cortex for intratelencephalic neurons (commissural [COM] neurons; red). **(B)** The retrograde rAAV AAVrg-hSyn-EGFP was injected in the pons or contralateral mPFC to label CP or COM neurons, respectively. One CP (red) and one COM neuron (green) are shown in sagittal and horizontal views (images generated using the MouseLight interface; ID AA0261 and AA0656, https://www.janelia.org/project-team/mouselight/neuronbrowser). **(C)** Representative images and Imaris 3D rendering of basal dendrites from CP WT, CP *Itgb3* KO, COM WT and COM *Itgb3* KO LV pyramidal neurons. Arrows point to representative thin (T), mushroom (M) and stubby (S) spines. Loss of *Itgb3* reduces spine length in CP neurons. Intensity profiles of the same dendrites after straightening reveal a 'spine neck kink' only in the COM WT and COM KO conditions, suggesting that COM neurons (WT and KO alike) exhibit spines with thinner spine necks than CP neurons (WT and KO alike). **(D)** Left: sample Imaris 3D rendering of thin, stubby and mushroom spines. Right: pie chart of spine type distribution (*p = 0.03; ***p = 0.0003; Chi-square test; n = 482, 532, 476 and 317 spines for CP WT, CP *Itgb3* KO, COM WT and COM *Itgb3* KO, respectively). **(E)** Density of stubby spines (two-way ANOVA; genotype effect: F (1, 90) = 3.548, p = 0.0628; neuron type effect: F (1, 90) = 13.45, ***p = 0.0004; genotype x neuron type interaction: F (1, 90) = 2.670, p = 0.1057; n = 27, 17, 31 and 19 dendritic stretches for CP WT, CP KO, COM WT and COM KO, respectively). **(F)** Violin plot for the length of thin spines (*p = 0.01, non-parametric Kruskal-Wallis ANOVA followed by Benjamini, Krieger and Yekutieli post-test, which corrects for multiple comparisons by controlling the false discovery rate; n = 245, 276, 242 and 157 thin spines for CP WT, CP *Itgb3* KO, COM WT and COM *Itgb3* KO, respectively). In each violin plot, the thick dotted line and the two thin dotted lines indicate the median and the quartiles, respectively. **(G)** Thin spines of CP *Itgb3* KO neurons were ranked according to their length, resampled to match the number of thin spines of CP WT neurons and plotted against the ranked thin spines of CP WT neurons (straight line: CP WT vs. CP WT; open circles: CP *Itgb3* KO vs. CP WT; line through open circles is a sigmoid fit; p = 0.01; Kolmogorov-Smirnov test; n = 245 and 276 thin spines for CP WT and CP *Itgb3* KO, respectively; full data set in supplemental Fig. 2). **(H)** Histogram of the ratio between length and head width for thin spines of CP WT and CP *Itgb3* KO neurons on a logarithmic scale (Log (length / width)) reveals a log-normal distribution for this morphological parameter (**p = 0.004 between CP WT and CP *Itgb3* KO, parametric Brown-Forsythe and Welch ANOVA followed by Benjamini, Krieger and Yekutieli post-test; full data set in supplemental Fig. 2). Continuous lines are Gaussian fits with the indicated means (µ) and standard deviations (σ)

also largely asymmetric, with COM neurons projecting mostly unidirectionally to CP neurons, which, in turn, convey information outside the cortex [3, 15]. Alterations in dendritic spines specific to CP neurons may therefore compromise the computational output of the full cortex, thereby contributing to ASD pathophysiology.

**Abbreviations**

| | |
|---|---|
| ASD | Autism spectrum disorder |
| COM | Commissural |
| CP | Corticopontine |
| LV | Layer V |
| mPFC | Medial prefrontal cortex |
| retro-rAAV | Retrograde recombinant adeno-associated virus. |

## Supplementary Information

The online version contains supplementary material available at https://doi.org/10.1186/s13041-023-01031-z.

Supplementary Material 1

**Acknowledgements**
We thank Dr A. Thalhammer (UniTs) and members of the Cingolani Lab for helpful discussion and critical reading of the manuscript.

**Authors' contributions**
LC performed imaging and morphological analyses and wrote the manuscript. FJ performed immunostaining experiments and contributed to writing the manuscript. CV performed intracranial injections. LAC supervised the project, analyzed data, wrote the manuscript and provided funding. All authors have approved the final version of the manuscript.

**Funding**
This work was supported by the Compagnia San Paolo (proposal ID: 2015 0702 to LAC.), the Cariplo Foundation (proposal ID: 2019–3438 to LAC) and the ERC-Horizon-EIC-2022-Pathfinderopen-01-01 (proposal ID: 101099579 to LAC).

**Data Availability**
The datasets generated during and/or analyzed during the current study are available from the corresponding author.

## Declarations

**Ethics approval and consent to participate**
All experiments were performed in accordance with EU and Italian legislation.

**Consent for publication**
Not applicable.

**Competing interests**
The authors declare that they have no competing interests.

Received: 4 April 2023 / Accepted: 27 April 2023
Published online: 09 June 2023

**References**

1. Kasai H, Ziv NE, Okazaki H, Yagishita S, Toyoizumi T. Spine dynamics in the brain, mental disorders and artificial neural networks. Nat Rev Neurosci. 2021;22(7):407–22. https://doi.org/10.1038/s41583-021-00467-3.
2. Willsey HR, Willsey AJ, Wang B, State MW. Genomics, convergent neuroscience and progress in understanding autism spectrum disorder. Nat Rev Neurosci. 2022;23(6):323–41. https://doi.org/10.1038/s41583-022-00576-7.
3. Baker A, Kalmbach B, Morishima M, Kim J, Juavinett A, Li N, et al. Specialized subpopulations of deep-layer pyramidal neurons in the neocortex: bridging Cellular Properties to Functional Consequences. J Neurosci. 2018;38(24):5441–55. https://doi.org/10.1523/JNEUROSCI.0150-18.2018.
4. Tervo DG, Hwang BY, Viswanathan S, Gaj T, Lavzin M, Ritola KD, et al. A designer AAV variant permits efficient Retrograde Access to Projection neurons. Neuron. 2016;92(2):372–82. https://doi.org/10.1016/j.neuron.2016.09.021.
5. Belgard TG, Marques AC, Oliver PL, Abaan HO, Sirey TM, Hoerder-Suabedissen A, et al. A transcriptomic atlas of mouse neocortical layers. Neuron. 2011;71(4):605–16. https://doi.org/10.1016/j.neuron.2011.06.039.
6. Willsey AJ, Sanders SJ, Li M, Dong S, Tebbenkamp AT, Muhle RA, et al. Coexpression networks implicate human midfetal deep cortical projection neurons in the pathogenesis of autism. Cell. 2013;155(5):997–1007. https://doi.org/10.1016/j.cell.2013.10.020.
7. Jaudon F, Thalhammer A, Cingolani LA. Integrin adhesion in brain assembly: from molecular structure to neuropsychiatric disorders. Eur J Neurosci. 2021;53(12):3831–50. https://doi.org/10.1111/ejn.14859.
8. Carter MD, Shah CR, Muller CL, Crawley JN, Carneiro AM, Veenstra-Vanderweele J. Absence of preference for social novelty and increased grooming in integrin beta3 knockout mice: initial studies and future directions. Autism Res. 2011;4(1):57–67.
9. Jaudon F, Thalhammer A, Zentilin L, Cingolani LA. CRISPR-mediated activation of autism gene Itgb3 restores cortical network excitability via mGluR5 signaling. Mol Ther Nucleic Acids. 2022;29:462–80. https://doi.org/10.1016/j.omtn.2022.07.013.
10. Kerrisk ME, Cingolani LA, Koleske AJ. ECM receptors in neuronal structure, synaptic plasticity, and behavior. Prog Brain Res. 2014;214:101–31. https://doi.org/10.1016/B978-0-444-63486-3.00005.
11. Tonnesen J, Katona G, Rozsa B, Nagerl UV. Spine neck plasticity regulates compartmentalization of synapses. Nat Neurosci. 2014;17(5):678–85. https://doi.org/10.1038/nn.3682.
12. Swinehart BD, Bland KM, Holley ZL, Lopuch AJ, Casey ZO, Handwerk CJ, et al. Integrin β3 organizes dendritic complexity of cerebral cortical pyramidal neurons along a tangential gradient. Mol Brain. 2020;13(1):168. https://doi.org/10.1186/s13041-020-00707-0.
13. Riccardi S, Cingolani LA, Jaudon F. CRISPR-Mediated activation of alphaV integrin subtypes promotes neuronal differentiation of Neuroblastoma Neuro2a cells. Front Genome Ed. 2022;4:846669. https://doi.org/10.3389/fgeed.2022.846669.
14. Ning L, Tian L, Smirnov S, Vihinen H, Llano O, Vick K, et al. Interactions between ICAM-5 and beta1 integrins regulate neuronal synapse formation. J Cell Sci. 2013;126(Pt 1):77–89. https://doi.org/10.1242/jcs.106674.
15. Anastasiades PG, Carter AG. Circuit organization of the rodent medial prefrontal cortex. Trends Neurosci. 2021;44(7):550–63. https://doi.org/10.1016/j.tins.2021.03.006.

## Publisher's Note

## Supplemental information

# Regulation of dendritic spine length in corticopontine layer V pyramidal neurons by autism risk gene β3 integrin

**Lucia Celora[1, *], Fanny Jaudon[1, 2, *], Carmela Vitale[3] and Lorenzo A. Cingolani[1, 3, 4]**

[1] Department of Life Sciences, University of Trieste, 34127 Trieste, Italy

[2] IRCCS Ospedale Policlinico San Martino, 16132 Genoa, Italy

[3] Center for Synaptic Neuroscience and Technology (NSYN), Fondazione Istituto Italiano di Tecnologia (IIT), 16132 Genoa, Italy

[4] Correspondence: lcingolani@units.it

* These authors contributed equally to this study

## Supplemental figures

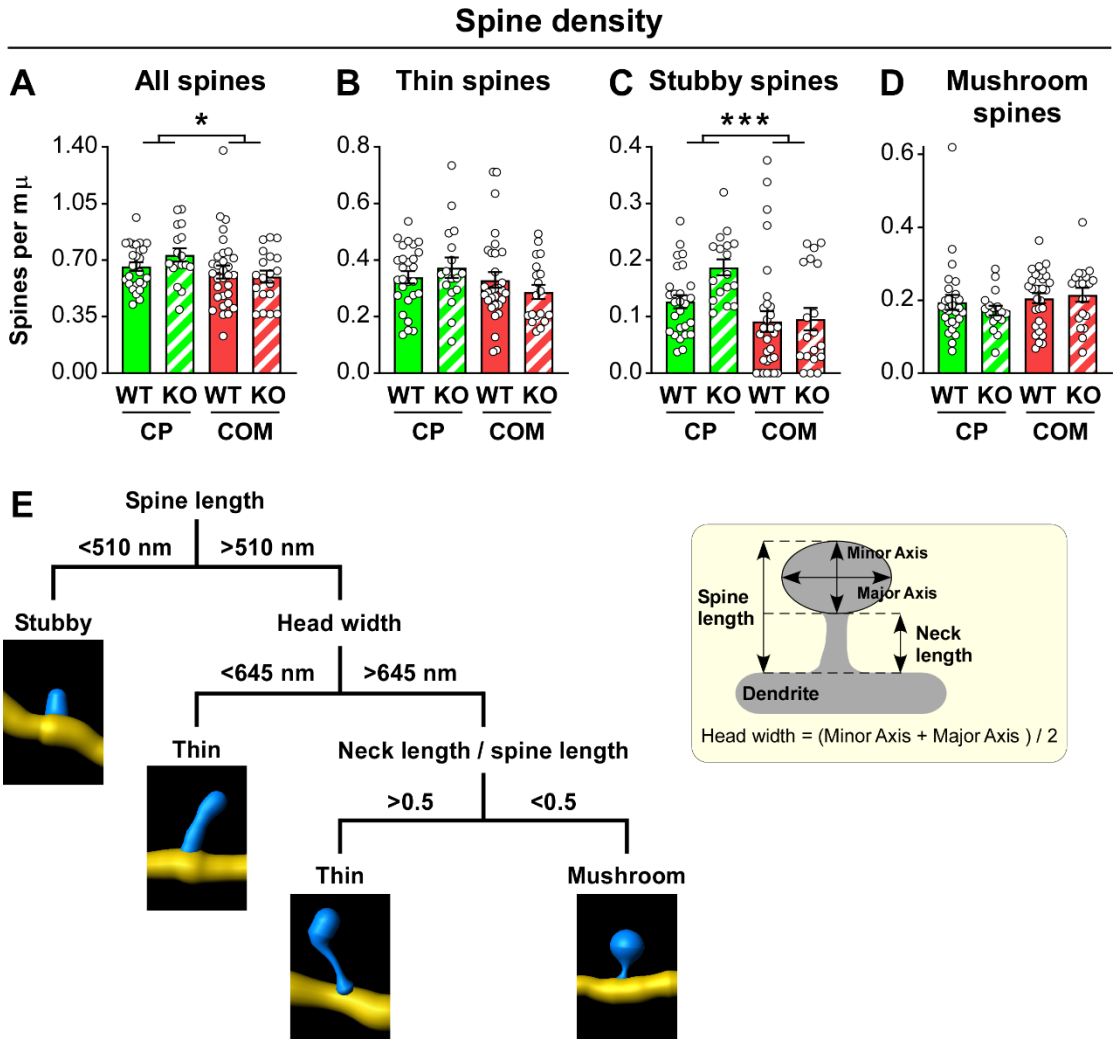


**Supplemental Figure 1. Dendritic spine density. (A)** Density of all dendritic spines (two-way ANOVA; genotype effect: F (1, 90) = 0.3154, p = 0.5758; neuron type effect: F (1, 90) = 4.746, *p = 0.032; genotype x neuron type interaction: F (1, 90) = 1.685, p = 0.1976; n = 27, 17, 31 and 19 dendritic stretches for CP WT, CP KO, COM WT and COM KO, respectively). **(B)** Density of thin spines (two-way ANOVA; genotype effect: F (1, 90) = 0.02147, p = 0.8838; neuron type effect: F (1, 90) = 2.819, p = 0.0966; genotype x neuron type interaction: F (1, 90) = 1.766, p = 0.1872). **(C)** Density of stubby spines; same data as in panel (E) of Fig 1 (two-way ANOVA; genotype effect: F (1, 90) = 3.548, p = 0.0628; neuron type effect: F (1, 90) = 13.45, ***p = 0.0004; genotype x neuron type interaction: F (1, 90) = 2.670, p = 0.1057). **(D)** Density of mushroom spines (two-way ANOVA; genotype effect: F (1, 90) = 0.1371, p = 0.7120; neuron type effect: F (1, 90) = 2.269, p = 0.1355; genotype x neuron type interaction: F (1, 90) = 0.7915, p = 0.3760). **(E)** Morphological criteria used for the classification of dendritic spines into stubby, thin and mushroom types.

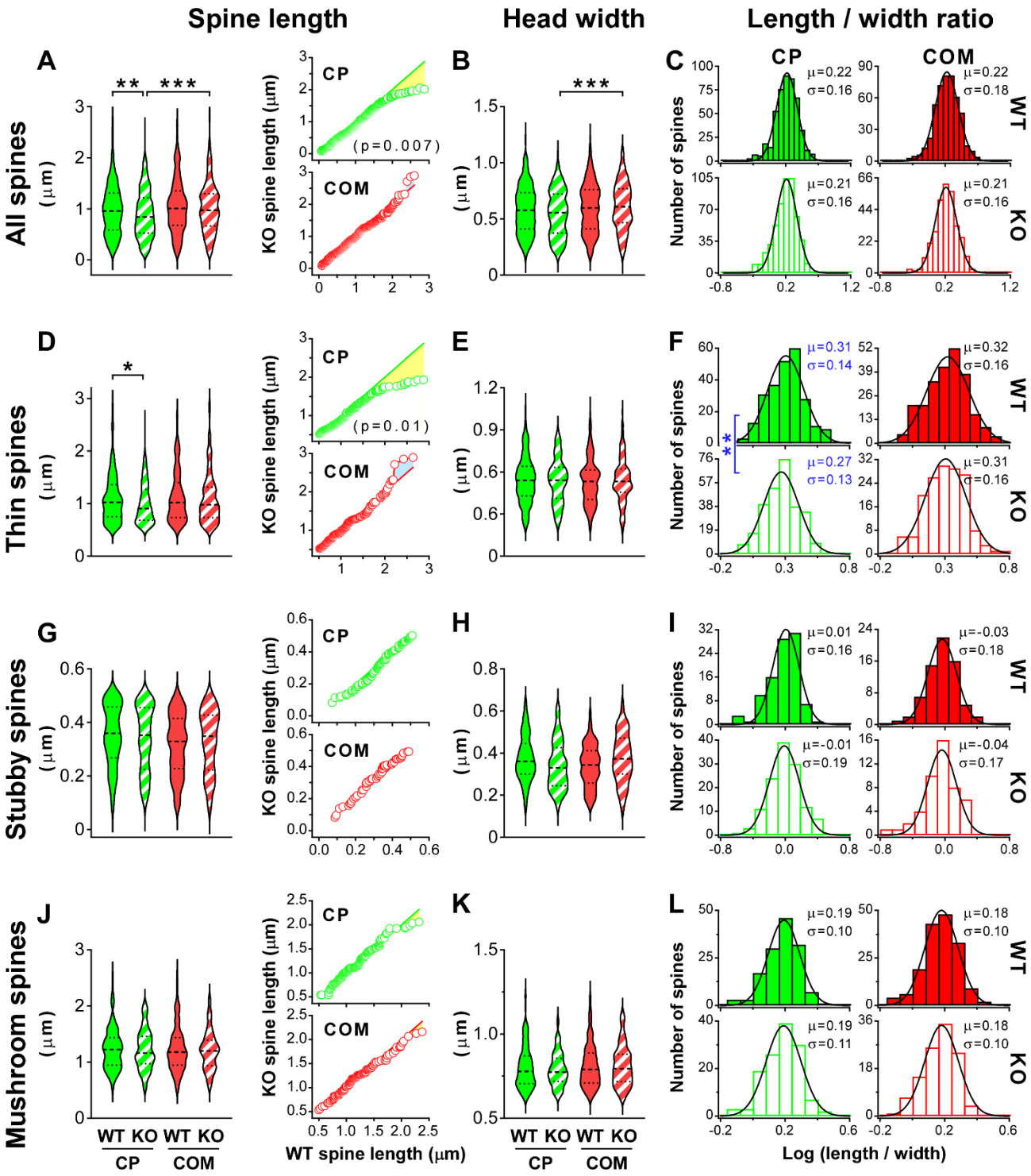


**Supplemental Figure 2. Length and head width of basal dendritic spines in corticopontine and commissural layer V pyramidal neurons from WT and *Itgb3* KO mice. (A)** Left, violin plot for the length of all dendritic spines (**p = 0.0043, ***p = 0.0004; non-parametric Kruskal-Wallis ANOVA followed by by Benjamini, Krieger and Yekutieli post-test, which corrects for multiple comparisons by controlling the false discovery rate). In each violin plot, the thick dotted line and the two thin dotted lines indicate the median and the quartiles, respectively. Right, all dendritic spines of CP *Itgb3* KO (top) or COM *Itgb3* KO

neurons (bottom) were ranked according to their length, resampled to match the number of dendritic spines of CP WT (top) or COM WT neurons (bottom) and plotted against the ranked dendritic spines of CP WT (top) or COM WT neurons (bottom). Straight green line: CP WT vs. CP WT; green open circles: CP *Itgb3* KO vs. CP WT; straight red line: COM WT vs. COM WT; red open circles: CP *Itgb3* KO vs. CP WT; p = 0.007; Kolmogorov-Smirnov test; n = 482, 532, 476 and 317 dendritic spines for CP WT, CP *Itgb3* KO, COM WT and COM *Itgb3* KO, respectively. **(B)** Violin plot for the head width of all dendritic spines (***p = 0.0002; non-parametric Kruskal-Wallis ANOVA followed by Benjamini, Krieger and Yekutieli post-test). **(C)** Histogram of the ratio between length and head width for all dendritic spines on a logarithmic scale (Log (length / width)). Continuous lines are Gaussian fits with the indicated means ($\mu$) and standard deviations ($\sigma$). **(D-F)** As in (A-C) but for thin spines. Left of panel (D), top right of panel (D) and left of panel (F) show the same data as panels (F-H) of Fig 1. (*p = 0.01 in left panel of (D), Kruskal-Wallis ANOVA followed by Benjamini, Krieger and Yekutieli post-test; p = 0.01 in top right panel of (D), Kolmogorov-Smirnov test; **p = 0.004 in (F), Brown-Forsythe and Welch ANOVA followed by Benjamini, Krieger and Yekutieli post-test; n = 245, 276, 242 and 157 thin spines for CP WT, CP *Itgb3* KO, COM WT and COM *Itgb3* KO, respectively). **(G-I)** As in (A-C) but for stubby spines (n = 98, 127, 70 and 48 stubby spines for CP WT, CP *Itgb3* KO, COM WT and COM *Itgb3* KO, respectively). **(J-L)** As in (A-C) but for mushroom spines (n = 139, 129, 164 and 112 mushroom spines for CP WT, CP *Itgb3* KO, COM WT and COM *Itgb3* KO, respectively).

## Materials and Methods

### Animals

All experiments were performed in accordance with EU and Italian legislation. *Itgb3* KO mice (B6;129S2-Itgb3tm1Hyn/J, Jackson Laboratory) were described previously (1-4) and were backcrossed to the C57BL/6j background >10 times at the time of experiments.

### Intracranial injections

Neurons projecting subcortically to the pons (corticopontine; CP) and intracortically to the contralateral cortex (commissural; COM) were labeled with EGFP by injecting the retrograde recombinant adeno-associated virus (retro-rAAV) AAVrg-hSyn-EGFP (1 µL; 1:5 dilution, titer: 1.5 x $10^{13}$ vg/mL, Cat. No. 50465-AAVrg, Addgene; (5)) into the pontine nuclei (A-P/M-L/D-V coordinates from Bregma: -4.16 / ±0.40 / 5.65 mm) and the contralateral prefrontal cortex (A-P/M-L/D-V coordinates from Bregma: 1.98 / + or -0.40 / 1.00 mm), respectively, at P28 (**Fig 1B**).

### Immunohistochemistry

Ten to fifteen days post-infection, mice were intracardially perfused with 4% paraformaldehyde (PFA). The brain was postfixed for 6 hrs in 4% PFA at 4°C and cryoprotected in 30% sucrose; 50 µm-thick coronal sections of the prefrontal cortex were cut with a Sliding Microtome (HM 430, ThermoFisher scientific). Sections were permeabilized in 0.3% TritonX-100 for 30 min, blocked with 10% normal goat serum (NGS) for 1 hr and then incubated with a chicken anti-GFP primary antibody (1:1000; Cat. No. AB13970, Abcam) for 2 hrs and an Alexa Fluor488-conjugated anti-chicken secondary antibody (1:500; Cat. No. A11039, ThermoFisher scientific) for 1 hr.

### Confocal microscopy and image analysis

Confocal stacks were acquired blind to the genotype with a Nikon Eclipse C1si using a 60x plan apochromat oil immersion objective (NA 1.40), 3x digital zoom, 0.96 µs pixel dwell time, 0.07 µm pixel size, 1 AU pinhole, 0.2 µm between optical sections and 3x scan averaging. Intensity of the 488 nm laser was set to 10 - 15% to achieve saturation of the somata and the PMT gain to 7 for all images.

We analyzed confocal images blind to the genotype using ImageJ. We filtered each stack using a Gaussian filter (radius: 0.5 pixels), Z-projected the maximal fluorescence intensities of in-focus stacks and applied the automatic ImageJ brightness/contrast. We analyzed dendritic spines in 17-31 regions of interests (ROIs), containing dendritic stretches of at least

10 µm long, from 3-4 different mice per condition. We excluded primary dendrites from the analysis and measured dendrite length across Z-stacks using the Neuroanatomy-SNT plugin of ImageJ (https://imagej.net/plugins/snt). In **Fig 1C**, intensity profiles were calculated after straightening the dendrites with the plugin Straighten (https://imagej.net/plugins/straighten) of ImageJ. The plugin SpineJ (6) of ImageJ was used to automatically identify dendritic spines and extract geometric information about the spines, namely length of the full spine (spine length), length of the spine neck (neck length) and width of the spine head (head width). For spine classification, we operationally defined (i) stubby spines as those with spine length <510 nm, (ii) mushroom spines as those with spine length >510 nm, head width >645 nm and neck length / spine length ratio <0.5, and (iii) thin spines as those with spine length >510 nm and either head width <645 nm or neck length / spine length ratio >0.5 (**Fig S1E**). 3D rendering was performed in Imaris 7.4 (Oxford Instruments).

### Statistical analysis

Statistical differences were assessed using the Chi-square test, the Kolmogorov-Smirnov test, the two-way analysis of variance (ANOVA), the Kruskal-Wallis ANOVA or the Brown-Forsythe and Welch ANOVA followed by the Benjamini, Krieger and Yekutieli post-test, as indicated (Prism 7; GraphPad Software).

### References


1. Cingolani LA, Goda Y. Differential involvement of beta3 integrin in pre- and postsynaptic forms of adaptation to chronic activity deprivation. Neuron Glia Biol. 2008;4(3):179-87. 10.1017/S1740925X0999024X.
2. Cingolani LA, Thalhammer A, Yu LM, Catalano M, Ramos T, Colicos MA, et al. Activity-dependent regulation of synaptic AMPA receptor composition and abundance by beta3 integrins. Neuron. 2008;58(5):749-62. 10.1016/j.neuron.2008.04.011.
3. Jaudon F, Thalhammer A, Zentilin L, Cingolani LA. CRISPR-mediated activation of autism gene Itgb3 restores cortical network excitability via mGluR5 signaling. Mol Ther Nucleic Acids. 2022;29:462-80. 10.1016/j.omtn.2022.07.013.
4. McGeachie AB, Skrzypiec AE, Cingolani LA, Letellier M, Pawlak R, Goda Y. beta3 integrin is dispensable for conditioned fear and Hebbian forms of plasticity in the hippocampus. Eur J Neurosci. 2012;36(4):2461-9. 10.1111/j.1460-9568.2012.08163.x.
5. Tervo DG, Hwang BY, Viswanathan S, Gaj T, Lavzin M, Ritola KD, et al. A Designer AAV Variant Permits Efficient Retrograde Access to Projection Neurons. Neuron. 2016;92(2):372-82. 10.1016/j.neuron.2016.09.021.
6. Levet F, Tønnesen J, Nägerl UV, Sibarita JB. SpineJ: A software tool for quantitative analysis of nanoscale spine morphology. Methods. 2020;174:49-55. 10.1016/j.ymeth.2020.01.020.